Projection of Sciences onto Textile And Fashion: Nano-Technology And Chargeable Fabric Example - Part II

Temel Bilimlerin Tekstil ve Moda Üzerine İzdüşümü: Nanoteknoloji ve Şarj Edilebilir Kumaş Örneği - II. Kısım

Deniz İYİDOĞAN[1], Özgür AKDEMİR[1], Jitka ERYILMAZ[1], Gökhan KAPLAN[1], Melda Birgül ÇAVUŞ[2], Mürşide HACIİSMAİLOĞLU[2], Mürsel ALPER[2], Özgür ÇOBANOĞLU[1]
[1]SANKO Tekstil İşletmeleri A.Ş., Bursa, Turkey
[2]Uludağ University, Physics Dep., Bursa, Turkey

Araştırma Makalesi / Research Article

PROJECTION OF SCIENCES ONTO TEXTILE AND FASHION: NANO-TECHNOLOGY AND CHARGEABLE FABRIC EXAMPLE - PART II

Deniz İYİDOĞAN[1]
https://orcid.org/0000-0003-3331-6514
Özgür AKDEMİR[1]
https://orcid.org/0000-0002-6352-1052
Jitka ERYILMAZ[1]
https://orcid.org/0000-0003-3839-8045
Gökhan KAPLAN[1]
https://orcid.org/0000-0001-8526-7051
Melda Birgül ÇAVUŞ[2]
https://orcid.org/0000-0003-3022-7620
Mürşide HACIİSMAİLOĞLU[2]
https://orcid.org/0000-0001-5648-3230
Mürsel ALPER[2]
https://orcid.org/0000-0001-8220-6851
Özgür ÇOBANOĞLU[1*]
https://orcid.org/0000-0002-6710-3691
[1]SANKO Tekstil İşletmeleri A.Ş., Bursa, Turkey
[2]Uludağ University, Physics Dep., Bursa, Turkey

ABSTRACT: This proceeding is the second part of a previous work, which provides readers with an overview of our multidisciplinary approach to technical textile research. It reviews the recent results of the project aiming at developing super-capacitor fabric structures. The fundamental idea of the project is based on, production of graphene nano-sheets and their application onto fabrics, growing the oxides of manganese on graphene coating and utilization of the final fabric within a suitable electrolyte as electrode material. After sample fabric weaving and battery cell preparation are briefly introduced, cyclic voltammetry and electro-impedance spectroscopy characterization of the fabricated samples are summariazed. Simple test circuit design for the measurements, basic micro-controller firmware development as well as data quality monitoring software application for visualization purposes are also introduced. Finally, the measurement results with over 800 F/g capacitance for graphite are presented.

Keywords: Super-capacitor, wearable technology, energy storage, battery

TEMEL BİLİMLERİN TEKSTİL VE MODA ÜZERİNE İZDÜŞÜMÜ: NANOTEKNOLOJİ VE ŞARJ EDİLEBİLİR KUMAŞ ÖRNEĞİ - II. KISIM

ÖZET: Bu metin, araştırma grubumuzun teknik tekstile olan çoklu-disiplin yaklaşımını, elektriksel olarak doldurulabilir kumaş geliştirme proje örneği üzerinden sunan çalışmanın ikinci kısmıdır. Bahsi geçen proje, grafen nano-yüzey üretimi, kumaşı oluşturan liflerin grafen nano-yüzeyler ile kaplanması ve bunların üzerinde manganez elementinin oksitlerinin büyütülmesi ile uygun bir elektrolit içinde elektrot malzemesi olarak kullanılması fikrine dayalı olarak kurgulanmıştır. Bu metinde, elektrot olarak kullanılacak kumaş örneklerinin dokunması, pil yapısının oluşturulması ve elektro-kimyasal olarak karakterize edilmesi özetlenmiştir. Metin, testler için geliştirilmesi gerekli devre tasarımı, sürücü ve veri kalitesi izleme yazılımı geliştirilmesi ve ölçüm sonuçlarının sunulması ile sonlanmıştır. Grafit için ulaşılan spesifik sığa 800 F/g olarak hesaplanmıştır.

Anahtar Kelimeler: Süper-kapasitör, giyilebilir teknoloji, enerji depolama, pil

1. INTRODUCTION

Fibers conformably coated with single atom thick nano-sheets of carbon, called graphene, are capable of isolating the surface of the fibres from their surroundings, upon which other nano-structures such as manganese oxides can be bound and construct a battery in multi-layer fabric form [1]. The graphene coating in this application, has dual functions i) act as the additive to bind other nano-structures and ii) makes the fabric electrically conductive. The conductance coupled with the growing pseudo-capacitive nano-crystals allows the fabric to function as an electrode material within a suitable electrolyte which might be formable by a slightly altered textile finishing process, forming a charge-able battery [2]. Pseudo-capacitance is utilized to increase the overall capacitance of the electrode material as we intend to maximize it.

For super-capacitors, transition metal oxides are being used as active electrode materials due to their low cost and natural abundance. The most common transition metal oxides utilized for this purpose are Ni-oxide [3], Co-oxide [4] and Mn-oxide [5]. Among them Mn-oxide is bio-compatible and has high theoretical capacitive value of about 1370 F/g [6]. Mn-oxides are generally grown in the form of thin films and nanowires by chemical or electrochemical deposition methods. By the electrochemical deposition, the structural properties of the deposits can be controlled better than those by the chemical deposition. In this work, in order to produce capacitive fabrics, steel yarns in addition to cotton yarns are used in fabric weaving, serving as one of the capacitive substrates and as current collector. Deposition is conducted on both the steel as well as on graphite coated cotton yarns to maximize the final total capacitance. For optimization of the deposition parameter, several tests were conducted and solution pH and temperature, deposition potential, charge amount and hence the Mn-oxide mass are all screened for higher capacitance of the final device.

In the first part of our work [1], we demonstrated the battery construction in multi-layer textile fabric form together with decision criteria for material selection as well as production method and characterization. In the second part of our work, we focus mainly on Mn-oxide deposition on both metal and carbon parts, electro-chemical characterization, firmware development and data quality monitoring tool development, all presented with detailed discussion. Overall, this study encapsulates the construction of the final capacitor and the development of the infrastructure for acquiring and for visualizing data.

2. MATERIALS AND METHODS
2.1 Materials

In this study super-capacitor was developed with three layers; two single electrodes in fabric form and a battery separator.

2.1.1 Single Layer Fabric as Electrode

A fabric was developed as a single electrode. Steel and graphene or carbon doped cotton materials were used for Mn-oxide deposition to form this electrode. A fabric sample, including indigo dyed cotton yarns in warp direction and both steel yarns and cotton yarns in weft direction, was woven with 3/1 left hand twill pattern. Steel yarns used in the construction were 100% stainless steel and purchased from Bekaert NV (Belgium). Sequence used in weft direction was 20 stainless steel yarns with 235 Tex and 5 cotton yarns with 20/1 Ne per 1 centimeter. Fineness of the yarn used for warp direction was 12/1 Ne with 27 thread/cm density. Total weight of the sample was 498,6g/m^2.

2.1.2 Battery Separator

After preparation of electrodes, solution of polyvinylidene flouride (PVDF, Kynar 761A, Arkema) in propylenecarbonate (PC) prepared as a gel electrolyte. Lithium hexafluoro phosphate (LiPF$_6$) added to PVDF solution to achieve ionic conductivity. Addition of LiPF$_6$ leads to sudden increase in viscosity. Increased viscosity was reduced upon stirring, as well-known thixrothropic behaviour. 20g PVDF, 60g PC, and 66mg LiPF$_6$, corresponding to w% of 0.33, are mixed into a gel electrolyte. Higher concentration of LiPF$_6$ leads to reduction of resistance or increase in conductivity; therefore, it is not used. In order to avoid electrode contact, aluminum oxide (Al$_2$O$_3$) coated non-woven polyester separator (Separion, from Evonik Industries) was used in fabric battery construction as separator.

2.1.3 Mn-Oxide Solution Preparation

MnSO$_4$.H$_2$O solution concentrations in the range from 0.01M to 1M are prepared for screening study. Actual deposition electrolyte solution is selected to be 0.5M for optimum pseudo-capacitance.

2.2 Methods

The details of each steps to form and analyse the fabric-form battery, to develop the infrastructure for acquiring data and visualizing them is presented as followings.

2.2.1 Mn-Oxide Deposition

The Mn-oxide for steel material was first deposited in a three electrode cell, for which the working electrode (i.e. substrate) was stainless steel sheet, the counter electrode was a Pt sheet and the reference electrode was a Saturated Calomel Electrode (SCE). The electrolyte was 0.5 M Mn-sulphate and the pH value was 5.0 whereas the depositions took place at room temperature, under a constant electrode potential in-between 1.5 to 2.5 V against SCE.

The chemical characterisation of the coating afterwards was carried out by a Fourier Transform Infrared (FTIR) spectroscopy, whereas capacitive behaviour was examined by Cyclic Voltammetry (CV) methods. The voltammograms were recorded in 0.5 M sodium-sulphate solution by varying electrode potential between 0 and 1 V against SCE at different scan rates such as 2, 5, 10, 30, 50 mV/s.

In order to simulate Mn-oxide growth on graphene, graphite rod electrodes were utilized as substrate first to demonstrate capacitance increment and then saturation of graphite surface by means of CV. After the parameter space was explored by chemical deposition of Mn-oxide on graphite surface and CV characterization of it, this time the graphene coating on cotton yarns was used as substrate and the results were confirmed.

2.2.2 Cell Preparation

Electrode fabric was structured as aforementioned in previous section and utilized as electrodes. They were cleaned with chemicals to remove waxes potentially picked-up during production. For wax removal, ethyl alcohol solution was applied for 1 minute, then washed with acetone and finally rinsed with water prior to overnight drying at 60˚C. Steel was used both as current collector and as substrate for nano-crystals to grow on, which was expected to provide extra pseudo-capacitance in addition to that of carbon-Mn-oxide layers. Cotton was utilized as the substrate for carbon coating on which Mn-oxide nano-crystals of the same type as those grown on steel were to be grown by thermal chemo-deposition. Fig. 1 shows the images of the electrode fabric before and after crystal growth by electro-deposition on steel, where the bright multifilament yarns are made of steel and the darker ones are cotton before carbon coating. Steel surface lost its shiny character due to electro-deposited Mn-oxide crystals, as seen from Fig. 1-A to B,

whereas cotton stays intact as electrodeposition has no effect on cotton as cotton was not yet made conductive by carbon coating. Carbon deposition by dipping followed by thermal chemo-deposition of Mn-oxide was applied as a later step on cotton to finalize the electrode structure. Similarly, chemical deposition of graphene on cotton has no effect on steel surface as neither an electrical potential difference was applied on the metal nor the nano-crystals grown on metal are soluble in the electrolyte.

Electrochemical deposition recipes of Mn-oxide on these fabrics were created based on the experiments conducted on stainless steel substrates. Electrochemical deposition experiments were conducted in 0.5 M aqueous solutions of $MnSO_4 \cdot H_2O$ and a DC power supply was used to deliver 2.9 V potential difference. Varying deposition times and concentrations in parallel cells as seen in Fig. 2 are followed in order to optimize crystal order and surface coverage.

2.2.3 Raman Spectroscopy for Crystal Characterization

In order to check whether the desired crystal is grown on steel surface, we utilized WiTec 300r confocal Raman imaging microscope with a single excitation laser wavelength of 532nm. 100x objective is used both for imaging as well as spectrum acquisition.
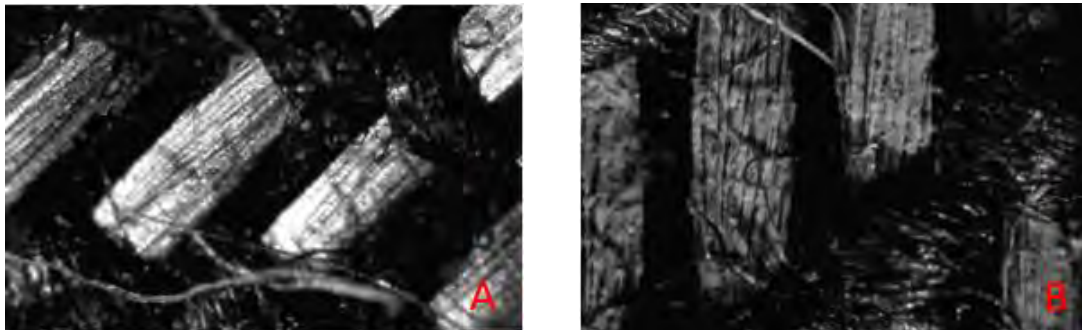

Figure 1. Optic microscope images of electrode fabric before (A) and after (B) crystal growth. Metallic bright colored yarns are steel and darker ones are carbon coated cotton. Note that electro-deposition works only on steel and no nano-crystal growth is observed on cotton.
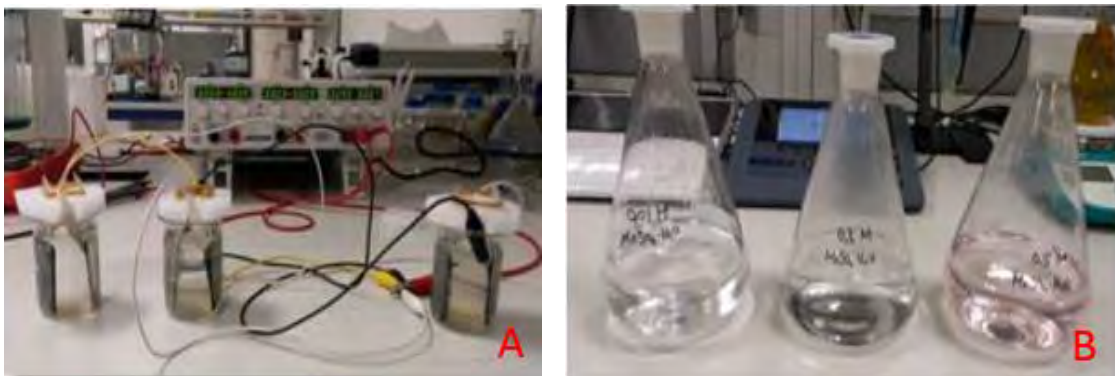

Figure 2. Three of deposition cells connected in parallel to DC power source during deposition process (A). $MnSO_4 \cdot H_2O$ solutions (B) are used for 30, 240, and 900 minutes of deposition process.

2.2.4 Electrochemical Characterization

In order to show capacitive behavior of steel and carbon via growing nano-crystals on their surfaces as well as to analyze the overall behavior of the final storage device in multi-layer fabric form, CV and EIS were used. Both the methods are known, widely utilized in the state of the art and finely detailed elsewhere [7].

We utilized a galvanostat-potentiostat PARSTAT-4000 from Princeton Applied Research with EIS add-on card included.

In Fig. 3 (a-b), impedance of a system plotted on imaginary axis as a function of frequency (a) and corresponding equivalent circuit model (b) are shown.

At low frequencies (i.e. mass transfer control), the system is modelled as a resistor and a capacitor in series and impedance drops down to the real axis as the frequency increases which in turn shorts the capacitance in series, hence reducing the total impedance of the system to that of the bare resistance in series vertically (i.e. 45-degree angle is due to Warburg resistance or impedance [8]). At high frequencies (i.e. kinetic control), the system behaves as a parallel configuration of a resistor and a capacitor, hence the shift from a near-linear to circular behavior. As the frequency increases, the impedance of the capacitor decreases. At some intermediate frequency, the impedance of the capacitor becomes equivalent to that of the resistor where current

is equally divided by both the parallel paths. This point corresponds to the middle of the circle. Therefore, the ideal model shown in Fig. 3-b can be fit onto the experimental data to extract the shown lumped components for further investigation of the system.

2.2.5 Test Circuit Design and Firmware Development

In order to generate I-V curves representing charge-discharge cycles of the final storage device in fabric form, that is, the Device Under Test (DUT), a simple analog electronic circuit controlled by an Arduino board is devised. Fig. 4-A depicts the analog circuit, where red ports are those connected to the Arduino pins for control (i.e. digital D5 and D6) and for potential and current measurements (i.e. analog A0, A1, and GND). Fig. 4-B shows the SPICE simulation wave forms with ideal components during the charge-discharge cycles of the DUT. The time constant of the node TAU is a function of the product of total DUT capacitance and discharge resistor R_1 in units of seconds and can directly be monitored as voltage decay on Fig. 4-B. Unit resistor R_2 (i.e. with value of 1 Ohm) is used to convert DUT current to voltage drop as the pin A1 is the input of a voltage-to-digital converter internally within the microcontroller.

The firmware development took place in standard Arduino Integrated Development Environment (IDE) and basically consists of reading out analog ports accordingly.
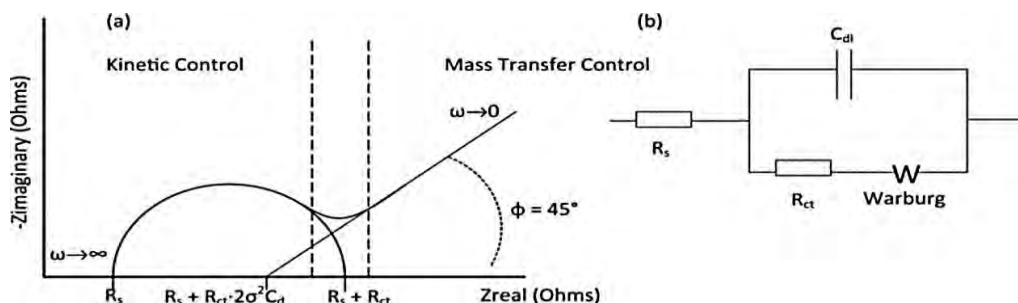

Figure 3: Characteristic shape of EIS measurement data for parameter extraction (a) and electronic model to fit, Randles equivalent (b)
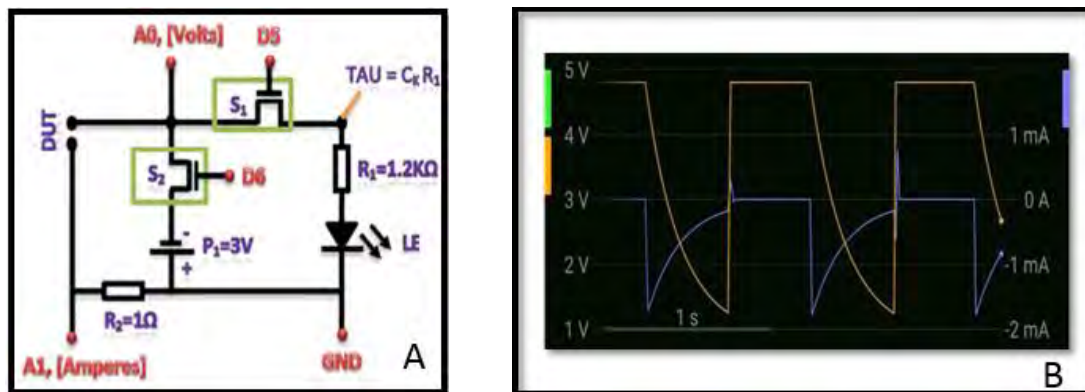

Figure 4. Functional schematic of charge/discharge circuit (A). Simulated I-V curves showing voltage across the DUT and its output current during charge/discharge cycles (B).

2.2.6 Development of a Data Quality Monitoring Tool

The measured data are acquired by the electronics as seen in Fig. 5-A and are sent to a computer for visualization (Fig. 5-B) and analysis. Such software tools are generally called Data Quality Monitors (DQM) developed for monitoring generated data usually in graphical form for ease of use. For this purpose, we developed a DQM tool utilizing processing programming language [9], running both on windows and Linux operating systems. The DQM tool reads out the Arduino board output via USB and visualizes the data on a screen as well as makes some basic calculations on the displayed data such as but not limited to calculating area-under-curve integrals for further analysis.

3. RESULTS AND DISCUSSION

The deposition potential was screened to measure the specific capacitive values of the Mn-oxide films. The maximum specific capacitive value was found for the samples produced at 1.5 V vs. SCE deposition potential. Fig. 6-A shows FTIR spectra of Mn-oxide film produced from the sulfate solution at room temperature under deposition potential of 1.5 V and with the charge amount of 0.1 C on steel substrate. The peaks seen in the range of 500-750 cm^{-1} belong to Mn-O bonds. The peaks appeared at the wavelengths greater than 1000 cm^{-1} represent O-H bonds. The Raman peaks seen in Fig. 6-B represent the alpha-phase of Mn-Oxide crystals.

Fig. 7-A and B display CV curves of bare stainless steel and Mn-oxide film on stainless steel, respectively. The mass of this film is 45 μg which is computed by Faraday's Law, assuming 100% current efficiency. In order to investigate whether carbon as an electrode material can have pseudo-capacitive behavior, we have grown 45 μg Mn-oxide nano crystals on a graphite rod and measured its CV before and after growth. Fig. 8 shows CV of graphite before A and after B nano-crystal growth. Note the resistive behavior before crystal growth as current changes with potential linearly just as in resistors. Capacitive behavior becomes evident after growth as the linear relationship between potential and current disappears and the characteristic capacitive relation takes place. Calculated specific capacitance values as seen in Fig. 11 are compatible with the literature reported elsewhere [5]. The specific capacitance of Mn-O on graphite was higher than that obtained for the film deposited on stainless steel. Likely, Mn-oxide/graphite structure behaves as a hybrid electrode and hence resulting in higher effective capacitance values.
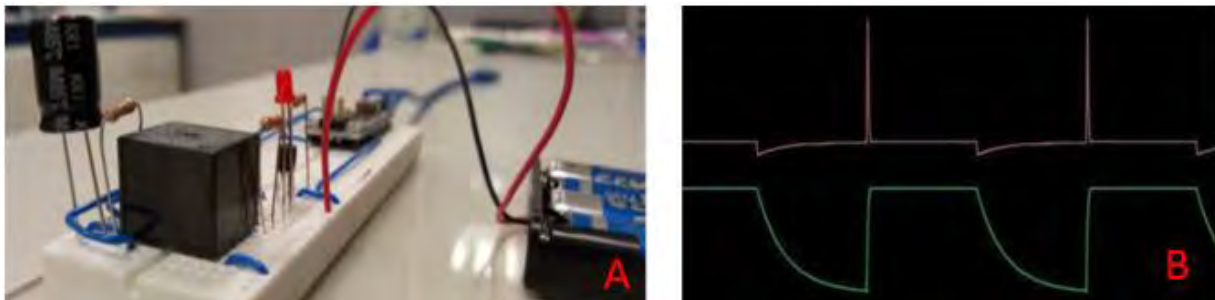

Figure 5. Circuit of Fig. 4-A on bread-board to characterize an electrolytic capacitor (i.e. black cylinder on the left (A)) and the display of DQM (B) visualizing cyclic DUT I-V curves being acquired during charge/discharge events. Note the similarity with the simulation of Fig. 4-B.
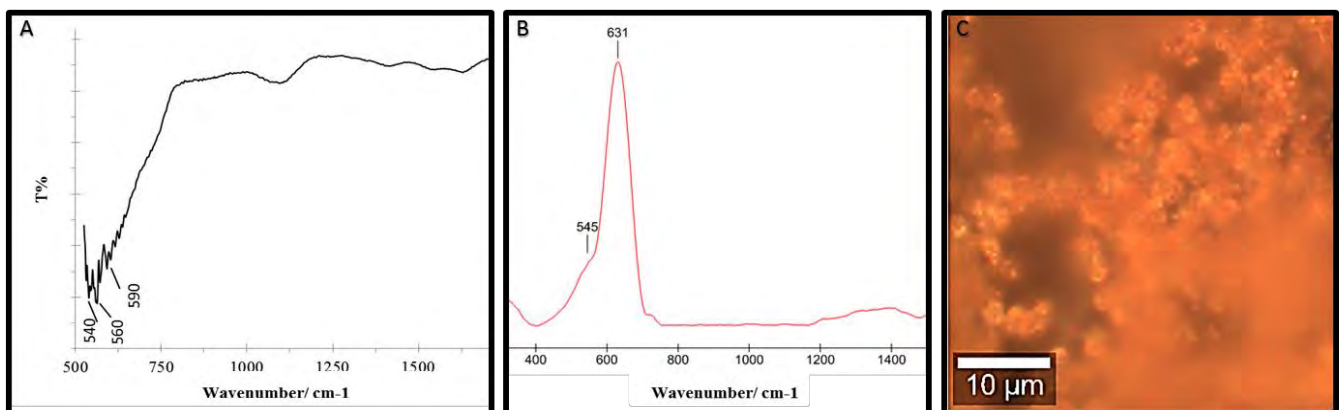

Figure 6. FTIR (A) and Raman (B) spectra of Mn-oxide coating developed in sulfate solution at room temperature under deposition potential of 1.5 V with a charge amount of 0.1 C in total. Corresponding confocal optic image (C) of nano-crystals of Fig. 1-B is also provided. Marked Raman peaks represent the alpha phase Mn-oxide crystals.
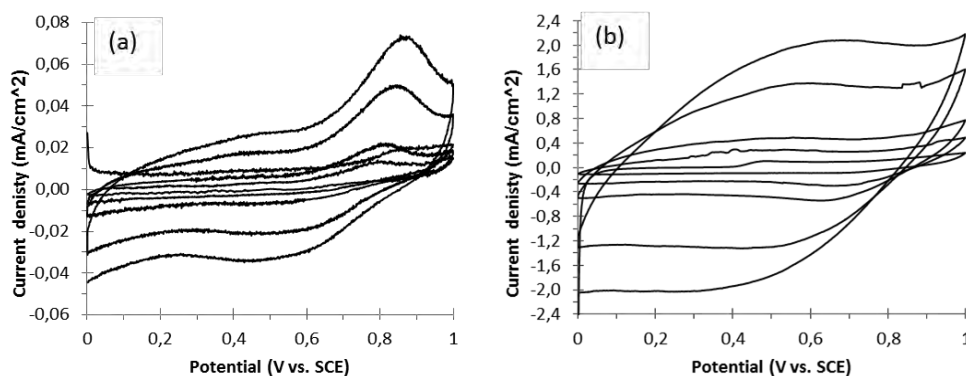
Figure 7. Cyclic voltammograms of stainless steel (a) and Mn-oxide film electrodeposited on stainless steel (b) for sweep rates of 2, 5, 10, 30 and 50 mV/s.
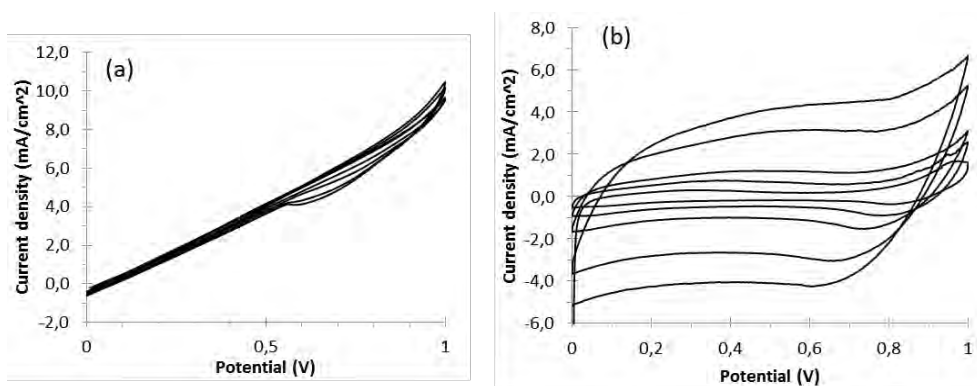

Figure 8. CV of graphite before (a) and after (b) nano-crystal growth for scan rates of 2, 5, 10, 30, 50 mV/s.

Electrodeposition of Mn-oxide on steel yarn surfaces was optimized as a function of $MnSO_4 \cdot H_2O$ concentration and deposition time (see Fig. 9-B). Each deposition condition was repeated three times for better understanding of experimental result deviations. For this reason, experimental set up having three parallel connected deposition cells, having electrode pairs submerged in solution with concentrations of 0.01M - 0.5M $MnSO_4 \cdot H_2O$, established as seen in Fig. 2-A. Separion separator and gel electrolyte prepared as shown in Fig. 10-C were used in between bare electrode and MnO_2 deposited electrode to construct the cell.

Fig. 9-A depicts the increment of final capacitance as a function of the amount of Mn-oxide grown on graphite rod. Mn-oxide deposition on carbon surface increases with deposition time as seen by data in red. Data in black belong to control solution in which Mn did not exist. Note slight capacity increment with time, possibly due to surface roughening during operation. It is also evident from the data in red that after roughly 20 minutes of deposition, the capacitance does not increase further possibly due to curtaining effect, even though, the amount of nano-crystals continues to increase. Fig.9-B plots capacitance as a function of deposition time and concentration of the deposition solution. Low concentration with long deposition results in higher capacitance, possibly due to more compact and controlled arrangement of nano-crystals.
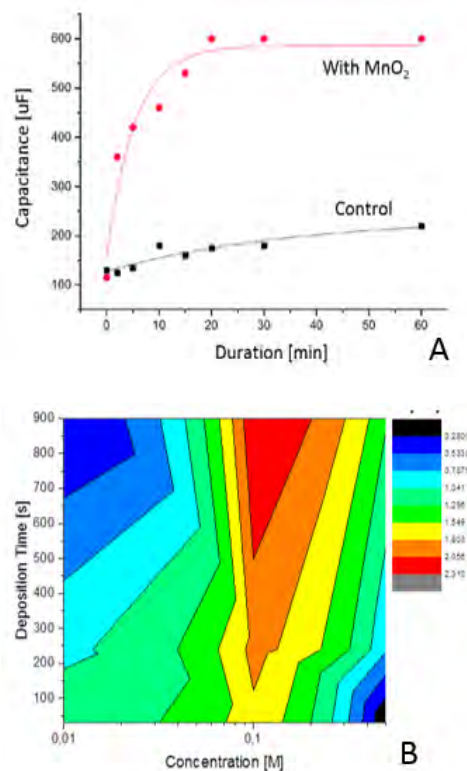

Figure 9. Capacitance of the DUT as functions of Mn-Oxide deposition duration (A) and deposition solution concentration (B).

Variation of complex resistance as a function of frequency, also known as Electro-Impedance Spectrum (EIS), is shown in Fig. 10-A in-between 10 Hz - 20 kHz for the sample depicted in the inlined image C. This data revealed long electrode-electrolyte effective path, value of Warbrug resistance, and many other parameters related to the fine interactions both at the current collector-electrode as well as electrode-electrolyte interfaces. Inlined plot B shows the measured potential across DUT (left y-axis) and output current (right y-axis) during charge/discharge cycle as a function of time. Noise in discharge current was due to loose connection. Fig. 10-C shows the final DUT construction where two individual fabrics were isolated by a separator within a gel electrolyte. This structure was used as two-terminal battery both for powering real-world applications as well as for EIS characterizations. The sample has roughly 3 cm^2 effective surface area. Since the geometric capacitance term and DUT's internal capacitance were not sufficiently different from each other as shown in Fig. 3, the impedance does not go all the way down to the real axis at intermediate frequencies. This was caused by the poor contact in-between the current collecting yarns and the electrolyte [10] through carbon-coated yarns due to intrinsic textile properties where the contact property of the aforementioned path was naturally not strong.

Power retention, defined as the capacity of a battery cell to preserve its loaded charge over time, was also measured to be low. This is attributed to the fact that electrode-electrolyte interface development on the electrode was not performed. Interface development is known to be a very important step which is kept outside of the scope of the work presented here. The process to develop an electrolyte-electrode interface constitutes an emphasized commercial know-how in battery industries.

4. CONCLUSIONS

A battery construction in multi-layer textile fabric form [1] together with all the fundamental steps to test it is presented. The stretchable textile battery exhibits 800 F/gr specific capacitance for graphite and 370 F/gr for steel as plotted in Fig. 11., which are close to the theoretical limit. Under actual load, the cell's maximum charge capacity, which is a standard for battery cell comparison, is measured to be 0.8 mAh for a 3cm^2 effective area. Charge capacity being proportional to the effective area of such a battery cell, this work clearly shows the potential of utilizing textile materials as electrical energy storage, especially in the wearable field as an emerging alternative to rigid batteries.

This developed potential was demonstrated by utilizing the small cell of Fig. 10-C to power up a real-world application (not shown in the image) in which an Atmel ATmega328P microcontroller is running a sequential LED light-up firmware. The device has 32kB flash, 2kB RAM, 1kB EEPROM, and consumes 1.2mA (typical) at 3V power supply, and has a clock frequency of 4MHz. The LED display sinks current levels of 1.5mA per LED at 3.0V and 5.0mA per LED at 5.0V, in total.

Sample fabric weaving and electro-chemical battery cell preparation methods are introduced; cyclic voltammetry and electro-impedance spectroscopy characterization of the fabricated battery cells in fabric form are detailed. Development of electronic characterisation infrastructure such as circuit design, firmware and data quality monitoring software development is also introduced. Finally, the corresponding measurement results, where high specific capacitance values close to the theoretical limits of Mn-oxide on graphite and steel substrates are summarized.
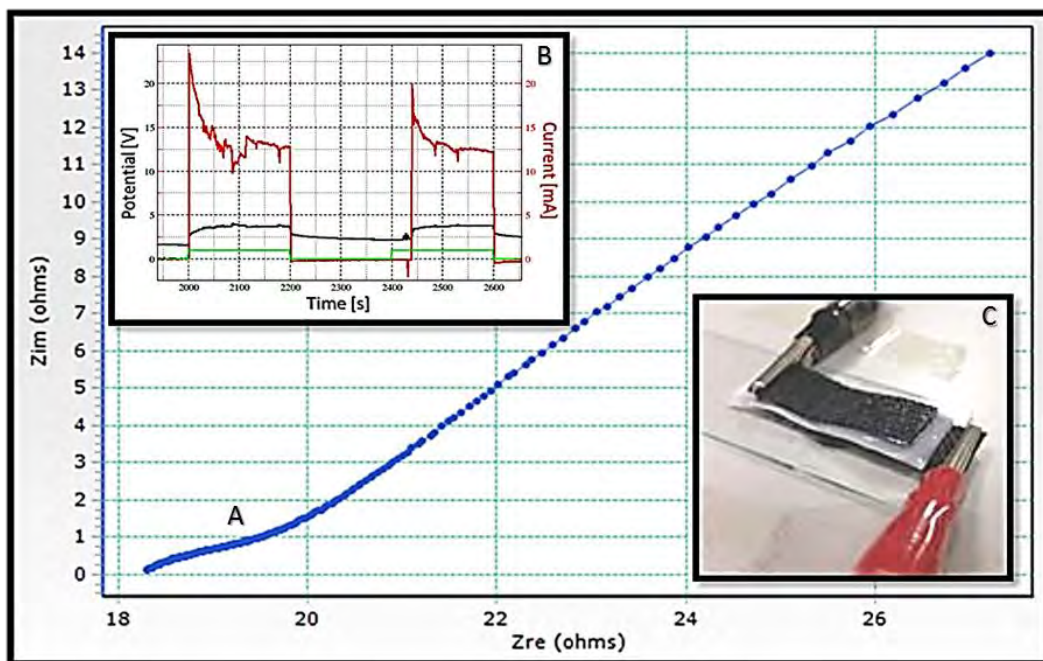

Figure 10. Measurement results and the sample cell on which the corresponding measurements were recorded.
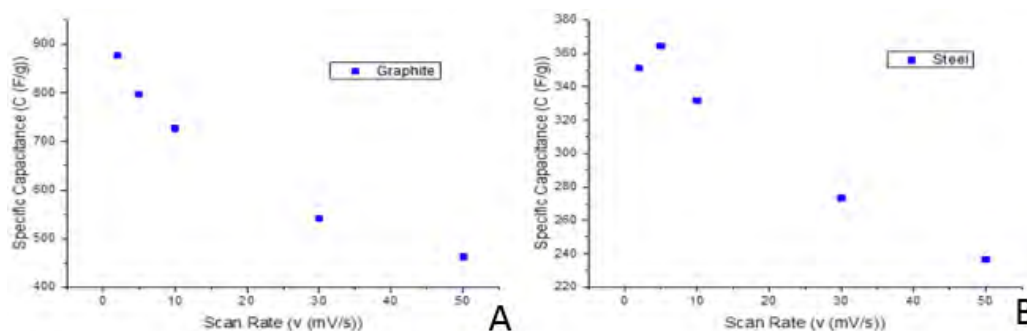
Figure 11: Specific capacitance values calculated for graphite (A) and steel (B) substrate for crystal growth.

This study illustrated that a fabric battery cell can be utilized to store electrical energy by the same phenomena as the commercially available batteries and also power a real-world application. It is expected that future research will even extend the range especially in terms of power retention which is on purposely kept outside the scope of this work. A fabric-based gel-electrolyte secondary battery has intrinsically better mechanical features compared to other types of batteries and this might play an important motivating role in the future studies.

As the battery presented here may have arbitrary shape and size, it might be a fashionable element in garment making rather than a fixed size rigid object that is to be hidden in a final product. Such a battery device can be distributed over a larger area such that it would not exhibit security concerns, against which regular batteries are tested, due to the fact that the stored power is distributed over a two-dimensional larger area compared to regular batteries. Since such an item may be part of a garment forming an integral section, it might well function as a *structural electronics,* hiding the actual function of energy storage and is utilized as base fabric. Therefore, a fabric battery might be the best manner generally for wearable energy storage devices to disappear in final products.

ACKNOWLEDGEMENTS

REFERENCES

1. Çobanoğlu Ö., Eryılmaz J., Ataşalan M. F., Kazanç S., (2015), *Projection of sciences onto textile and fashion: nano-technology and chargeable fabric example*, Tekstil ve Mühendis, 22: 97, 21-30.

2. Chen, S., Zhu, J., Wu, X., Han, Q., Wang, X., (2010) *Graphene Oxide-MnO^2 nanocomposites for supercapacitors*, ACS Nano, 4: 5, 2822-2830.

3. Paulose, R., Mohan, R. and Parihar, V. (2017). *Nanostructured nickel oxide and its electrochemical behaviour—A brief review*. Nano-Structures & Nano-Objects, 11, 102-111.

4. Mei, J., Liao, T. and Sun, Z. (2018). *Two-dimensional metal oxide nanosheets for rechargeable batteries*. Journal of Energy Chemistry, 27:1, 117-127.

5. Wang, J., Kang, F., Wei, B., (2015), *Engineering of MnO^2-based nanocomposites for high-performance supercapacitors*, Progress in Materials Science 74 51–124

6. Toupin M., Brousse T., Be´langer D., (2004), *Charge Storage Mechanism of MnO^2 Electrode Used in Aqueous Electrochemical Capacitor*, Chemistry of Materials, *16,* 3184-3190.

7. Allen, J. and Faulkner, L. (2000). *Electrochemical Methods: Fundamentals and Applications*. 2nd ed., ISBN: 13 978-0-471-04372-0

8. Huggins, R. (2009). *Advanced Batteries*., ISBN: 978-0-387-76424-5

9. Processing.org. (2017). *Processing.org*. [online] Available at: https://processing.org/ [Accessed 25 June 2017].https://processing.org/

10. Lukowics, P., Kirstein, T., Tröster, G., (2004), *Wearable Systems for Health Care Applications*, Schattauer Publishers, Methods Archive, 43:3, 232-238.